Advantages of Hybrid Neural Network Architectures to Enhance Prediction of Tensile Properties in Laser Powder Bed Fusion

Florian Funcke[1,2,a*], Tobias Forster[1,3,b], Peter Mayr[2,c]

[1]BMW Group FIZ, Knorrstraße 147, 80788 Munich, Germany

[2]Technical University of Munich, Chair of Materials Engineering of Additive Manufacturing, Boltzmannstraße 15, 85748 Garching b. Munich, Germany

[3]Ludwig-Maximilian-University Munich, Chair of Experimental Physics – Laser Physics Centre for Advanced Laser Applications, Am Coulombwall 1, 85748 Garching b. Munich, Germany

[a]florian.funcke@bmw.de, [b]t.forster@physik.uni-muenchen.de, [c]peter.mayr@tum.de

Abstract. The properties of AlSi10Mg produced by Laser Powder Bed Fusion (PBF-LB) are defined by a multitude of different machine and laser parameters. This multi-parameter space presents the challenge of optimizing the material properties for a given application by the sheer amount of possible parameter combinations. Characterizing this multi-parameter space empirically is limited by time and resources and thus yields an incomplete picture of the process capabilities and local optima, respectively. To improve on this situation, machine learning to map the process parameters on the tensile properties of AlSi10Mg was used. The Hybrid Neural Network (HNN) used in this study consisted of a Convolutional Neural Network (CNN) to process the micrographs and a Dense Neural Network (DNN) to process the LPBF process parameters as well as the output of the CNN. The micrographs given to the CNN part of the network were printed with the same parameters given to the DNN part to include the information of the bulk microstructure as it strongly influences the tensile properties of the material. With the HNN, we observed good accuracy of the predicted tensile properties, given the small amount of training data. Furthermore, we explore which features of the micrographs were extracted by the CNN.

Introduction

Laser Powder Bed Fusion (PBF-LB) offers great freedom to additively manufacture both complex 3D shapes and a variety of different materials with AlSi10Mg as one of the most common Aluminium alloys. The laser process itself offers highly customizable parameters which affect the resulting materials properties [1]. However, the amount of possible parameter combinations renders the global process optimization a highly demanding task, which requires both a lot of resources and time. In this context, machine learning was reported to offer a data-driven approach to optimization [2-3]. Liu et al. [4] demonstrated the benefits of ML, by modelling the relative density with respect to laser power and laser scan speed to obtain suitable process parameters. Furthermore, mechanical properties were determined with those parameters and linked to the corresponding microstructure captured with SEM at 12000x magnification and EBSD imaging.

Since relative density is not the most relevant material characteristic from an industrial standpoint, it might be advantageous to model mechanical properties directly. Furthermore, easy-to-obtain microstructure features could enhance the model's performance by adding relevant information. To determine which features would be suitable – other than global density/ porosity - we use machine learning (ML) to map the LPBF process parameters to mechanical properties after printing using a hybrid neural network architecture. It combines a Convolutional Neural Network (CNN) to extract microstructure features with a Dense Neural Network, which incorporates the scalar process parameters. The feature maps of the first convolutional layer were analyzed to yield relevant microstructure features.

Materials and Methods

Sample Manufacturing. For this study, two build jobs were printed on the machine SLM 500, equipped with two lasers, by SLM Solutions Group AG to create the data for machine learning. Gas-atomized AlSi10Mg powder was used as the feedstock. In total, 50 parameter combinations were chosen, and for each combination, a density cube of 10 mm x 10 mm x 10 mm and three tensile specimens with the geometry A4x20 according to DIN 50125 were printed.

Table 1. Variation of hatch, contour, and fill line parameters.

Parameter	Hatch	Contour	Fill line
Laser power P_L [W]	300-700	233-580	350
Laser scan speed v_L [mm/s]	500-3000	628-1400	600, 800
Laser spot diameter d_B [μm]	116.4-137.5	116.4	116.4
Scan distance s [mm]	0.15-0.23	0.17-0.20	0.20

The specimens were built by scanning in stripes and a subsequent rotation of 67° in each layer. Both the hatch and contour parameters were randomly varied (see Table 1) to achieve good distribution of parameters for the ML-model to learn. The fill line parameters were kept constant, except for its laser scan speed for three parameters which were an artefact of previous trials. Each build job used a different layer thickness of 50 μm and 100 μm, respectively. The build platform temperature was kept at 200 °C for each job, and nitrogen was used as shielding gas.

Sample Characterization. The mechanical properties of the printed samples were determined according to DIN EN ISO 6892-1 on the testing machine AllroundLine Z100 with robotic testing system roboTest L by ZwickRoell GmbH & Co. KG. The micrographs of the density cubes were taken on a light microscope Leica DM6 M with the camera Gryphax NAOS by Jenoptik AG at 25x magnification and stitched together to yield an image of the entire cross-section.

Image Preparation. Before training, images were transformed to a grayscale format to remove colour artefacts on the learning procedure. Afterwards, a local contrast enhancement was performed by means of the CLAHE-algorithm with the aim of equalizing image brightness and enhancing contrast [5]. It was implemented in Python with OpenCV [6] with 'cliplimit' set to 2.0 and 'tileGridSize' equal to (16,16). Furthermore, all images were scaled down in resolution to 1024 x 1400 and a center crop of size 256 x 256 was taken. Hereby, computational requirements could be met without losing a significant amount of micrograph information.

Available Data. With the 50 parameter combinations, 148 valid tensile tests were conducted and for every specimen, yield Strength $R_{p0,2}$, Ultimate Tensile Strength R_m and Elongation at Break A were evaluated. These values served as the target values we tried to predict with the HNN. As input parameters for the HNN, the laser power and scan speed for both hatch and contour, the hatch laser diameter and hatch distance, as well as layer thickness, were used.

Moreover, we used five dimensionless hatch parameters as additional input to increase the information content of the physical laser-material-interaction, derived from Patel et al. [7] (Eq. 1-5):

dl. Laser Power:
$$q^* = \frac{AP}{r_B \lambda (T_m - T_0)} \tag{1}$$

dl. Energy Input:
$$E^* = \frac{q^*}{v^* l^*} \tag{2}$$

dl. Layer Thickness:
$$l^* = \frac{2l_t}{r_B} \tag{3}$$

dl. Heat Input:
$$Q^* = \frac{q^*}{l^*} \tag{4}$$

dl. Velocity:
$$v^* = \frac{v r_B}{\alpha} \tag{5}$$

Hybrid Neural Network Architecture. A hybrid neural network (HNN) architecture was constructed that combined a Dense Neural Network and a Convolutional Neural Network to use micrograph images and process parameters simultaneously as input. All networks were built in Python with PyTorch [8].

Table 2. Hyperparameters of the Hybrid Neural Network.

Hyperparameter	Value
Hidden Activation Function	Leaky ReLU
Output Activation Function	Linear
Number of Filters	4, 8, 16
Convolutional Kernel Size	(7,7)
Convolutional Stride	(2,2)
Maxpooling Kernel Size	(2,2)
Maxpooling Stride	(2,2)
Optimizer	AdaMax
Batch Size	8
Learning Rate	0.02
Weight Decay	0.002
Reduced Learning Rate	Factor: 0.5, Patience: 50

The convolutional network part consists of alternating convolutional and maxpooling layers, with batch normalization after each pair of layers. Results of the convolutional part of the network were flattened and concatenated with a layer of the Dense Neural Network. In total, three pairs of convolutional and maxpooling layers were utilized and fed into a dense layer with eight neurons. The first hidden layer of the Dense Neural Network also consists of eight neurons resulting in 16 inputs for the next hidden layer after concatenating. Subsequently, another hidden layer with eight neurons processed the data before passing it to the output layer consisting of one neuron. Batch normalization was additionally used after each dense layer of the network. A sketch of the hybrid architecture is shown in Fig. 1 with corresponding hyperparameters provided by Table 2. With the aim of improving weight optimization of the HNN, the learning rate was reduced on plateau. This means that once no major decrease of test loss was present anymore for a certain number of time steps (patience), the learning rate was reduced by a fixed factor to increase chances of approximating a minimum of the loss function. Learnable biases were used as well.
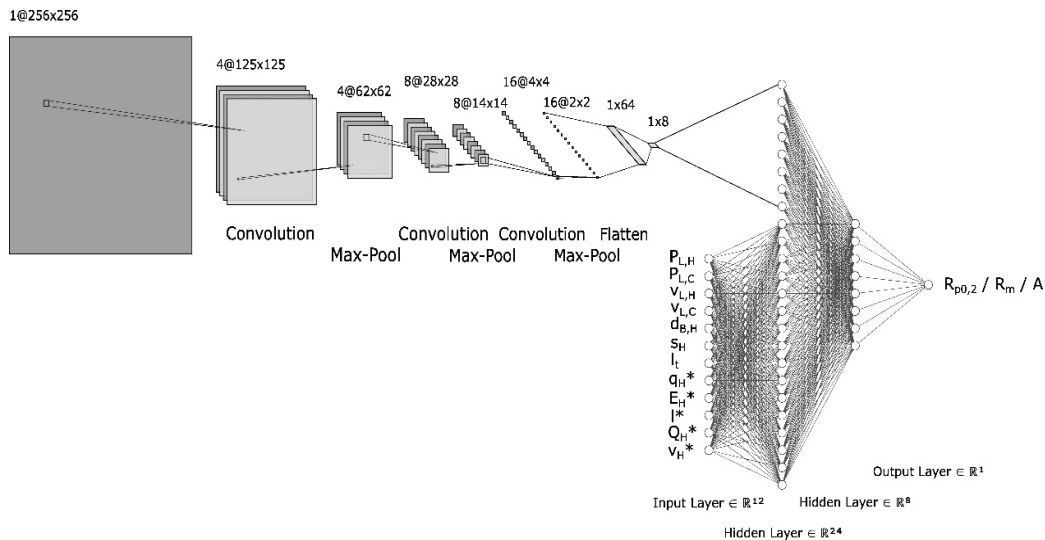

Fig. 1. Hybrid Neural Network Architecture.

Model Evaluation. To assess the model's performance, the Mean Absolute Error (MAE) and the Coefficient of Determination R^2 were used. The MAE offers the mean deviation of the model's prediction from the real data [9]. The Coefficient of Determination R^2 yields the fit of the model to the real data [10]. The model optimization pursues to maximize R^2 between 0 and 1 and to minimize the MAE simultaneously. 4-fold cross-validation was applied, and the results were averaged. The model was trained for 500 epochs and the epoch with best test metrics was chosen for evaluation.

Results

Prediction Accuracy. Fig. 2 depicts the results for the HNN on each target value. It predicts yield strength with a coefficient of determination of $R^2_{test} = 0.78$ and an Error of $MAE_{test} = 13.1$ MPa for the test set (training: $R^2_{train} = 0.81$, $MAE_{train} = 13.6$ MPa). For ultimate tensile strength the HNN delivers a slightly better fit with $R^2_{test} = 0.83$ but also a higher error of $MAE_{test} = 22.9$ MPa for testing (training: $R^2_{train} = 0.80$, $MAE_{train} = 25.3$ MPa). The HNN performs worst for elongation at break with $R^2_{test} = 0.69$ and $MAE_{test} = 0.66$ % (training: $R^2_{train} = 0.86$, $MAE_{train} = 0.46$ %). Compared to the training metrics, yield strength shows little, and ultimate tensile strength no overfitting. For elongation the HNN overfits noticeably with $R^2_{train} = 0.80$ for training compared to the test set. Qualitatively, the HNN delivers good prediction accuracy for both lower and higher strength values. The HNN also predicts values for elongation rather consistent across its range, with a slightly higher deviation for larger values. They were, however, much more spread out, compared to the strength values, as the metrics suggested. It can be assumed that the Elongation at break is more sensitive to additional influences, e.g., residual stresses, different surface roughness or imperfections, or general noise inherent to tensile testing. Overall, the HNN prediction for Elongation at Break could be improved upon. However, it delivers usable predictions for the Yield and Ultimate Tensile Strength, given the small dataset.
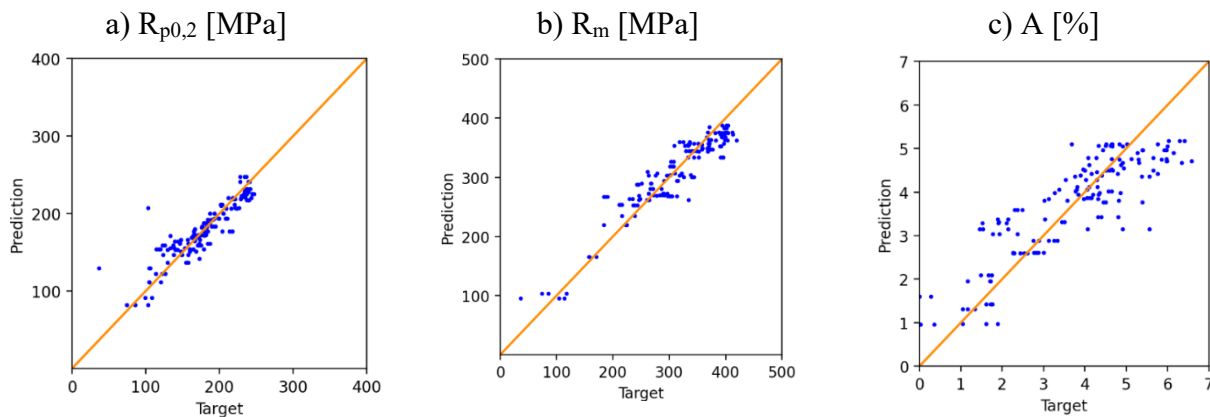
a) $R_{p0,2}$ [MPa]   b) R_m [MPa]   c) A [%]

Fig. 2. Test results of the HNN model, a) yield strength, b) ultimate tensile strength, c) elongation at break.

Feature Map Interpretation. To analyze which microstructural features were extracted by filters of the HNN, outputs of the first convolutional layer are shown in Fig. 3 and 4. Deeper hidden layers were not visualized due to the decreased resolution, which were hard to interpret. To generate the feature maps, the micrograph images were passed through the first layer of filters and the activation function before being normalized between 0 and 1 for plotting. Three representative images were chosen with little to high amounts of porosity. By means of filtering, the network detected contours, edges and areas which appeared as contrast in the feature maps. The used colormaps displayed small outputs as dark, interpreted as less relevant, and large outputs as light, interpreted as more relevant.

Fig. 3 shows the feature maps of all four filters of the first convolutional layer in the case of yield strength prediction. As the results of the model's fit indicate, the HNN predicted yield strength and ultimate tensile strength almost identically well. Their feature maps were also mostly identical in our

qualitative analysis. Thus, merely the feature maps of yield strength are presented in this study, being representative for both strength values.

The feature maps of image a) filter 1 displays a dark noisy image with a slight indication of the horizontal layer structure. Regarding image b) and c), more pore focused characteristics were observed. Here, high contrast edges between pores and the surrounding material were visible, which was especially pronounced for the high porosity image c). Filter 2 yielded a rather soft and noisy image focused on the solid material. The weld bead structure is recognizable in example image b), yet the porosity is not highlighted specifically. Filter 3 and 4 showed similar feature extraction characteristics. The horizontal layer structure of image a) was highlighted by these filters. Additionally, weld bead structures are recognizable in the image b). Especially filter 3 highlighted local contrasts between individual weld beads. Porosity was not emphasized by these two filters, as observed by image b) and c).
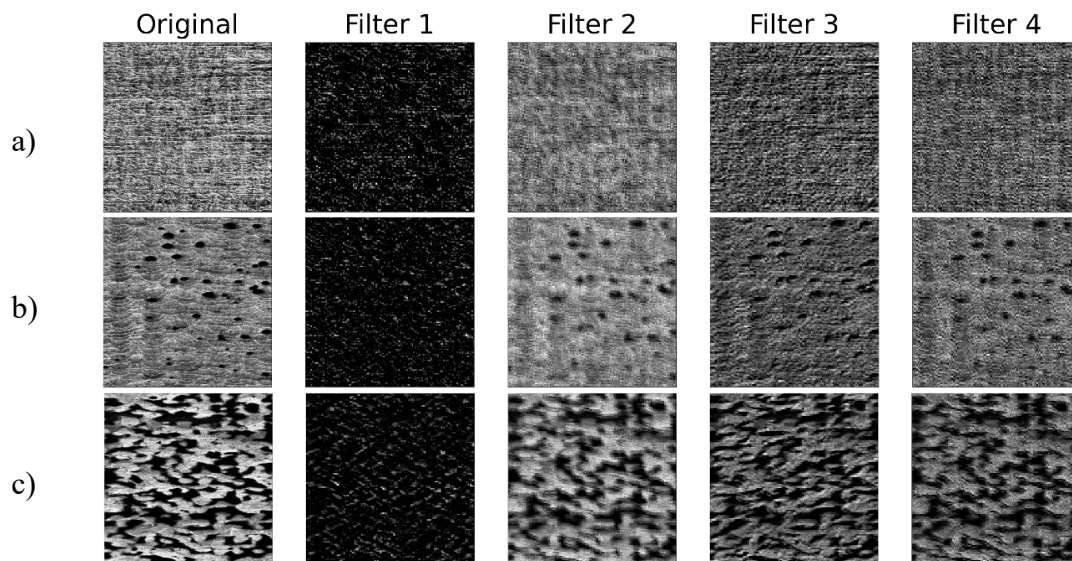

Fig. 3. Feature maps yield strength; a) low, b) medium, c) high porosity, image plane parallel to build direction.
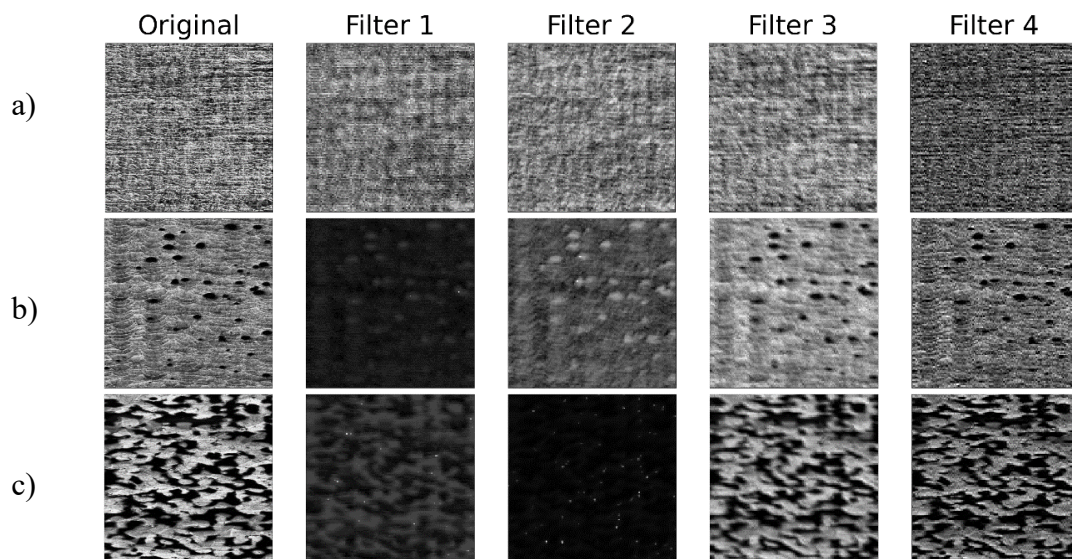

Fig. 4. Feature maps elongation at break; a) low, b) medium, c) high porosity, image plane parallel to build direction.

For Elongation at Break (Fig. 4) the feature maps 1-4 for image a) showed similar local contrasting of the layer structure of the material, which is comparable to image a), filter 3 of yield strength prediction. For image b) and c) filter 1 highligh-ted pores, as they appeared white with dark sur-roundings in example. A few pixels are very bright, which we interpreted as noise, yet which led to

a reduced total brightness of the images due to the normalization. Filter 2 depicts a comparable pore extraction for image b), in image c) bright-ness peaks of some pores are so pronounced, that the rest of the image appeared black. Filters 3 and 4 focus more on the solid material, and especially filter 4 depicts the layered structure of the material.

Conclusion

This study demonstrates that a Hybrid Neural Network delivers sufficient prediction of tensile properties, given the parameters of the LPBF process, dimensionless process parameters and corresponding micrographs. In detail, the results show the following:

- Yield and ultimate tensile strength can be modelled with > 80% accuracy and reasonably small errors evenly across the entire target value spectrum.

- Elongation at break was less accurately predicted with $R^2_{test} = 0.69$, which was significantly lower compared to the strength values. Yet the error was relatively low, with $MAE_{test} < 1\%$. It seems that elongation is more sensitive to additional influences and noise, which is information, the input data lacked.

- Considering the small amount of data, the HNN did not experience severe overfitting for the strength values, when comparing the training metrics against the test set. Elongation, however, was more affected by overfitting and would benefit from improved or higher amounts of data.

Furthermore, the feature map analysis reveals that meaningful microstructure features were interpretable from the first convolutional layer, which can be summarized as the following:

- Yield and Tensile strength show very similar feature extraction. For both targets, the HNN extracted the layer structure and weld beads, as well as the edges of pores present.

- For elongation at break, the layer structure and weld beads were highlighted. Regarding the porosity, entire pore areas were visible in the feature maps, instead of pore contours.

- It should be mentioned, that in following convolutional steps, the feature maps are suspect to further convolution, which could also inverse the feature maps and thus alter the extracted features. However, taking the pore contours into account, which are a prominent feature of high contrast change, this may seem to be unlikely, yet remains to be proved.

The findings of the feature maps prompt the question, of whether conventionally measured scalar microstructure features could be used as additional input parameters instead of the CNN-part of the network. Here we suggest using the following features for future experiments:

- For strength prediction, the actual layer thickness and weld bead geometries can be extracted, both as a global mean value or as a distribution. Additionally, the sphericity or sphericity distribution could be used to add porosity information.

- To augment the model for Elongation at break, actual layer thickness and weld bead geometries could be used analogously to the strength values. However, it seems to be advantageous to use the global porosity and the pore size distribution for the Elongation at Break.

References

[1] K. Riener et al.: Influence of particle size distribution and morphology on the properties of the powder feedstock as well as of AlSi10Mg parts produced by laser powder bed fusion (LPBF), Additive Manufacturing 34 (2020)

[2] Meng, L. et al. Machine learning in additive manufacturing: a review. JOM 72, 2363–2377 (2020)

[3] Jiang, M., Mukherjee, T., Du, Y. & DebRoy, T. Superior printed parts using history and augmented machine learning. npj Computational Materials 8, 184 (2022)

[4]   Liu, Q. et al. Machine-learning assisted laser powder bed fusion process optimization for AlSi10Mg: New microstructure description indices and fracture mechanisms. Acta Materialia 201, 316–328 (2020).

[5]   Zuiderveld, K., VIII.5. - Contrast Limited Adaptive Histogram Equalization, in: P. S. Heckbert, (ed.), Graphics Gems, Academic Press, 1994, pp. 474–485

[6]   G. Bradski, The OpenCV Library, Dr Dobb's Journal of Software Tools, 2000

[7]   Patel, S. & Vlasea, M. Melting modes in laser powder bed fusion. Materialia 9, 100591(2020).

[8]   A. Paszke,et al., Pytorch: An imperative style, high-performance deep learning library, in: H. Wallach et al. (eds.), Advances in neural information processing systems 32, 2019, pp. 8024-8035

[9]   Johnson et al.: Invited review: Machine Learning for materials development in metals additive manufacturing, Additive Manufacturing 36 (2020)

[10] Rahaman et al. : Machine Learning to Predict the Martensite Start Temperature in Steels, Metallurgical and Materials Transactions A, 2019